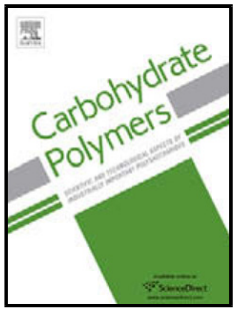

Structural heterogeneities in starch hydrogels

Todor T. Koev (Investigation) (Formal analysis) (Writing - original draft) (Visualization), Juan C. Muñoz-García (Investigation) (Methodology) (Writing - review and editing), Dinu Iuga (Resources) (Methodology), Yaroslav Z. Khimyak (Conceptualization) (Supervision) (Funding acquisition) (Writing - review and editing), Frederick J. Warren (Conceptualization) (Supervision) (Funding acquisition) (Writing - review and editing)

PII: S0144-8617(20)31007-9

DOI: https://doi.org/10.1016/j.carbpol.2020.116834

Reference: CARP 116834

To appear in: *Carbohydrate Polymers*

Received Date: 20 April 2020

Revised Date: 14 July 2020

Accepted Date: 26 July 2020

Please cite this article as: Koev TT, Muñoz-García JC, Iuga D, Khimyak YZ, Warren FJ, Structural heterogeneities in starch hydrogels, *Carbohydrate Polymers* (2020), doi: https://doi.org/10.1016/j.carbpol.2020.116834

Self-assembly properties of carboxylated tunicate cellulose nanocrystals prepared by ammonium persulfate oxidation and subsequent ultrasonication

Jintao He[a,b,1], *Kaiqiang Bian*[a,b,1] *and Guangzhe Piao*[a,b*]

[a] Key Laboratory of Rubber-plastics, Ministry of Education/Shandong Provincial Key Laboratory of Rubber-plastics, Qingdao University of Science & Technology (QUST), Qingdao 266042, China

[b] School of Polymer Science and Engineering, QUST, Qingdao, 266042, China

[1]These authors contributed equally to this work

Tel.: +86-0532-84022725; Fax: +86-532-840-22725

E-mail address: piao@qust.edu.cn (G. Piao)

Highlights:

- Carboxylated *t*CNCs with uniform nanoscale dimensions were successfully prepared.
- The formation of carboxylated *t*CNCs lyotropic N*-LCs was observed for the first time.
- The critical concentration of phase separation for *t*CNCs suspension was 3.5

wt%.

Abstract

Tunicate cellulose, extracted from the marine animal, has drawn increasing attention as the high crystallinity and aspect ratio. However, it is hard to prepare tunicate cellulose nanocrystals (*t*CNCs) with narrow size distribution in the traditional way, especially for the carboxylated samples, which also affects their lyotropic liquid crystal behavior to a certain extent. Herein, carboxylated *t*CNCs with uniform nanoscale dimensions and high surface charges density were prepared through ammonium persulfate (APS) oxidation and ultrasonic post-processing. Of particular interest, the formation of carboxylated *t*CNCs lyotropic chiral nematic liquid crystals was observed for the first time, which displayed obvious birefringence and fingerprint texture. Meanwhile, it was found that the critical concentration of phase separation for *t*CNCs suspension was around 3.5 wt% from the phase diagram. This study provides an efficient way to fabricate carboxylated *t*CNCs, and the self-assembly properties may lead to great potential applications in constructing advanced functional materials.

Keywords: tunicate; cellulose nanocrystals; carboxylation; chiral nematic liquid crystals; ultrasonic post-processing

1. Introduction

The concept of green sustainability runs through the development of present society, which also promotes the rapid development of renewable and degradable

environmental-friendly materials. Cellulose nanocrystals (CNCs), a class of fascinating bio-based nanoscale materials, have attracted a tremendous amount of interest in recent decade due to its unique structural features and impressive physicochemical properties (Chen et al., 2018; Thomas et al., 2018; Trache, Hussin, Haafiz, & Thakur, 2017). The unique self-assembly properties make CNCs a valuable chiral template, by combining with other materials, it is possible to develop fascinating photonic materials that can be used for sensing, anti-counterfeiting, or decoration (Kelly, Giese, Shopsowitz, Hamad, & MacLachlan, 2014; Tran, Boott, & MacLachlan, 2020). As a reinforcing filler, CNCs can substantially enhance the mechanical properties of the polymer by forming a percolated network within the polymer matrix (Miao & Hamad, 2019). Besides, CNCs also provide a wide range of applications such as oil/water separation (Cheng, Ye, Chang, & Zhang, 2017), drug delivery (Wang, He, Zhang, Tam, & Ni, 2015), metallic reaction templates (Kaushik & Moores, 2016), etc.

As is well known, cellulose has a large number of active hydroxyl groups on the surface. To be useful for applications, however, it is often necessary to modify the hydroxyl groups in a way that changes their surface chemistry. There are now many ways to realize the modification, and among them, carboxylation of CNCs is a typical representative, which can provide more active sites and display excellent thermal stability compared with traditional acid hydrolysis (Liu et al., 2020). Several methods including TEMPO mediated oxidation (Isogai, Saito, & Fukuzumi, 2011), ammonium persulfate (APS) oxidation (Leung et al., 2011), periodate-chlorite oxidation

(Suopajärvi, Liimatainen, Hormi, & Niinimäki, 2013), $KMnO_4$ oxidation (Zhou et al., 2018), citric/hydrochloric acid hydrolysis (Yu, Chen, Wang, & Yao, 2015) and alkaline periodate oxidation (Liu et al., 2019; Nyström, Arcari, Adamcik, Usov, & Mezzenga, 2018) have been used to extract carboxylated CNCs from various biomass resources. In recent years, APS oxidation method has received much attention owing to the simple preparation and post-treatment process that avoids the difficulties of using and recycling concentrated sulfuric acid. Through a simple and versatile one-step procedure, APS can defibrillate and remove amorphous cellulose effectively, resulting in carboxylated CNCs with nanoscale dimensions (Leung et al., 2011; Oun & Rhim, 2018).

One of the interesting properties of the CNCs aqueous suspension is its ability to self-organize into liquid crystalline arrangement. Marchessault et al. (Marchessault, Morehead, & Walter, 1959) discovered CNCs suspension can display birefringence. Furthermore, Revol et al. demonstrated that CNCs generated by sulfuric acid hydrolysis in fact form chiral nematic liquid crystals (N*-LCs) (J. F. Revol, Bradford, Giasson, Marchessault, & Gray, 1992) and the alignment of nanocrystals can be affected by the external magnetic field (J. F. Revol et al., 1994). Upon reaching a critical concentration, the CNCs suspension will separate two phases with upper isotropic phase and lower anisotropic phase. Interestingly, the latter displays a chiral nematic structure that consisted of stacked planes of CNCs aligned along a director, with the orientation of each director rotated about the perpendicular axis from one plane to the next (He, Liu, Li, & Piao, 2017; Pan, Hamad, & Straus, 2010). It is

currently established that rod-like colloidal particles form nematic structures as a consequence of entropically driven self-orientation, which is based on the balance between translational entropy and orientational entropy (Azzam, Heux, & Jean, 2016; Schütz et al., 2018; Van Rie et al., 2019). In addition, the helical structure can be retained in solid films by evaporation-induced self-assembly, thus enabling intriguing photonic properties (J. F. Revol, Godbout, & Gray, 1998).

Tunicates are marine invertebrate sea animals that are revealed as the only animal source for cellulose. Large numbers of tunicate species are available in nature and the storage is tremendous, making it an excellent source of cellulose (Moon, Martini, Nairn, Simonsen, & Youngblood, 2011; Trache et al., 2017). High crystallinity is one of the significant characteristics of tunicate cellulose, and tunicate CNCs (*t*CNCs) have an almost pure crystalline form of I_{β}. Meanwhile, the large aspect ratio and excellent mechanical properties further expand its application (Sacui et al., 2014). For example, a tunicin whisker/plasticised starch nanocomposite material has been developed by Dufresne et al (Anglès & Dufresne, 2000, 2001). In addition, Li et al. (Zhao, Zhang, Lindström, & Li, 2015) prepared *t*CNCs/glucomannans nanocomposite films, which exhibit good thermal, optical and mechanical properties. However, there are few reports on the lyotropic liquid crystals behavior of *t*CNCs, especially the carboxylated samples. Kimura et al. (Kimura et al., 2005) found that *t*CNCs suspension (2.2 wt%) prepared by sulfuric acid hydrolysis underwent phase separation in about 10 days. Upon application of the horizontal field, highly regular monodomains were obtained. However, the helical axes would be unwound when

applying a rotating magnetic field. Habibi et al. (Habibi, Chanzy, & Vignon, 2006) observed non-uniform birefringence from aqueous *t*CNCs with carboxyl group obtained by TEMPO oxidation but failed to find the phase separation and the characteristic texture of fingerprint. This phenomenon may be ascribed to high polydispersity of the length (from 0.1 to 10 μm) of *t*CNCs and high viscosity of the suspensions. Usually, the high crystallinity of tunicate cellulose makes it hard to prepare *t*CNCs with uniform nanoscale dimensions, which also affects their assembly to a certain extent.

Therefore, the aim of this study was to prepare carboxylated *t*CNCs with narrow size distribution through APS oxidation and high-power ultrasonic post-processing, and further investigate their lyotropic liquid crystal behavior including phase transition and self-organization. In the study, the formation of lyotropic N*-LCs of carboxylated *t*CNCs was observed for the first time. This finding may bring new insight in the understanding of the self-assembly behavior of these systems that could be beneficial for the design of *t*CNCs based functional materials and the development of abundant tunicate resources (Chu et al., 2019; Chu et al., 2017).

2. Experimental section

2.1. Materials

Tunicate (*Halocynthia roretzi*, Rongcheng, China), cotton cellulose (Whatman CF11, UK), potassium hydroxide (Yantai Sanhe Chemical Reagent Co. Ltd., China), sodium hypochlorite solution (Tianjin Bodi Co. Ltd., China), glacial acetic acid (Tianjin Fuyu Fine Chemical Co. Ltd., China), ammonium persulfate (Tianjin Beichen

Founder Reagent Co. Ltd., China), phosphotungstic acid and polyethylene glycol (M_w=20000) (Sinopharm Chemical Regent Co. Ltd., China). All chemicals were of analytical grade, and water was distilled before use.

2.2 Preparation of the carboxylated *t*CNCs suspension

Tunicate cellulose was extracted from the mantle of *Halocynthia roretzi* through several times of alkali treatment and bleaching processes based on the previous report (Zhang, Zhang, Gao, & Piao, 2013). Afterwards, an aqueous carboxylated *t*CNCs suspension was prepared from tunicate cellulose mainly by following the APS oxidation method (Leung et al., 2011; Oun & Rhim, 2017). Meanwhile, little modification was adopted in the preparation process. Briefly, 2.0 g tunicate cellulose powder was mixed with 200 mL APS solution (2 mol/L), stirred and refluxed at 60° C for 16 h in a three-necked flask. The suspension was then diluted with 400 mL of deionized water to terminate the reaction and allowed to settle overnight. The clear supernatant was decanted and the remaining cloudy was repeatedly centrifuged at 10000 rpm to obtain a thick white suspension. In particular, the obtained suspension was further ultrasonically treated at 450 W for 30 minutes to decrease the sample size, then placed into dialysis membrane tubes (MWCO = 8000-14000) and dialyzed against de-ionized water for about one week. The resulting sample was concentrated by osmotic compression using a 10 wt% polyethylene glycol solution, and finally carboxylated *t*CNCs suspension with a concentration of 7.4 wt% was obtained. Meanwhile, carboxylated cotton CNCs (*c*CNCs) were also prepared by using the same method.

2.3 Preparation of *t*CNCs N*-LCs and iridescent film

The 7.4 wt% *t*CNCs suspension was diluted to 1.5, 2.4, 3.0, 3.5, 4.2, and 6.5 wt%, respectively, and then sonicated at 50 W for 30 min to enhance the dispersion. Finally, the samples were sealed in glass cuvettes and stored at 4℃to ensure the completion of self-assembly process.

5 mL of 3 wt% carboxylated *t*CNCs suspension was cast in 35 mm diameter polystyrene petri dishes and allowed to dry for 4 days under ambient condition. Thus, solid film was obtained.

2.3. Characterizations

Fourier transform infrared (FT-IR) spectra were collected with a 4 cm^{-1} spectral resolution by using Bruker VERTEX 70 spectrometer in the range of 4000-500 cm^{-1}. X-ray diffraction (XRD) measurements for the dried powder were carried out on Rigaku D/MAX-2500/PC diffractometer using Cu Kα radiation (λ = 0.154 nm). The diffraction signals were recorded in the range of 2θ = 5-50° with a step interval of 0.02° and a scanning rate of 5° min^{-1}. The crystallinity index (CrI) was calculated by the following equation:

$$CrI = (I_{200} - I_{amorphous}) / I_{200} \times 100\% \qquad (1)$$

where I_{200} is the intensity of the (200) lattice plane at $2\theta = 22.8°$, and $I_{amorphous}$ represents the intensity of amorphous phase at $2\theta = 18°$ (Reddy & Yang, 2005). In addition, the crystallite size of *t*CNCs was calculated out by Scherrer equation (French & Santiago Cintrón, 2013). The morphology and size distribution of *t*CNCs were analyzed using JEOL JEM-2100 transmission electron microscope (TEM),

where a droplet of dilute *t*CNCs suspensions (0.01 wt %) was dropped and stained (3 wt% phosphotungstic acid) on a copper grid before measurement. The dimension of *t*CNCs was analyzed by using Nano Measurer software version 1.2, and 150 samples were measured. Dynamic light scattering (DLS) and Zeta potential were measured on a Malvern Nano ZS90 light scattering instrument at a concentration of 0.01 mg mL^{-1} with Zetasizer analyzer. Polarizing optical microscope (POM) micrographs were taken from Leica DM2500P optical microscope equipped with a CCD camera and crossed polarizers. Samples of the nanocrystals suspensions for optical microscopy were placed in rectangular glass cuvettes. UV-Vis spectrum was measured with Shimadzu UV-2550 spectrophotometer. The film was placed in a test cell, and air was used as the reference. The carboxyl content of *t*CNCs was determined via conductometric titration. The *t*CNCs sample (dry weight 35 mg) was suspended into 50 mL of 0.01 M HCl solution. After 10 min of stirring, the suspension was titrated with 0.04 M NaOH. The carboxyl group content can be calculated from titration curve and therefore determine the degree of oxidation (DO) by the following equation:

$$DO=\frac{162 \times N \times (V_2 - V_1) \times 10^{-3}}{M - 36 \times N \times (V_2 - V_1) \times 10^{-3}} \qquad (2)$$

where (V_2–V_1) is the amount of NaOH (mL) required to deprotonate the carboxylic acids, N is the concentration of NaOH (mol/L), M is the weight of oven-dried sample (g), and the value of 36 corresponds to the difference between the molecular weight of an anhydroglucose unit and that of the sodium salt of a glucuronic acid moiety (Habibi et al., 2006; He et al., 2017).

3. Results and discussion

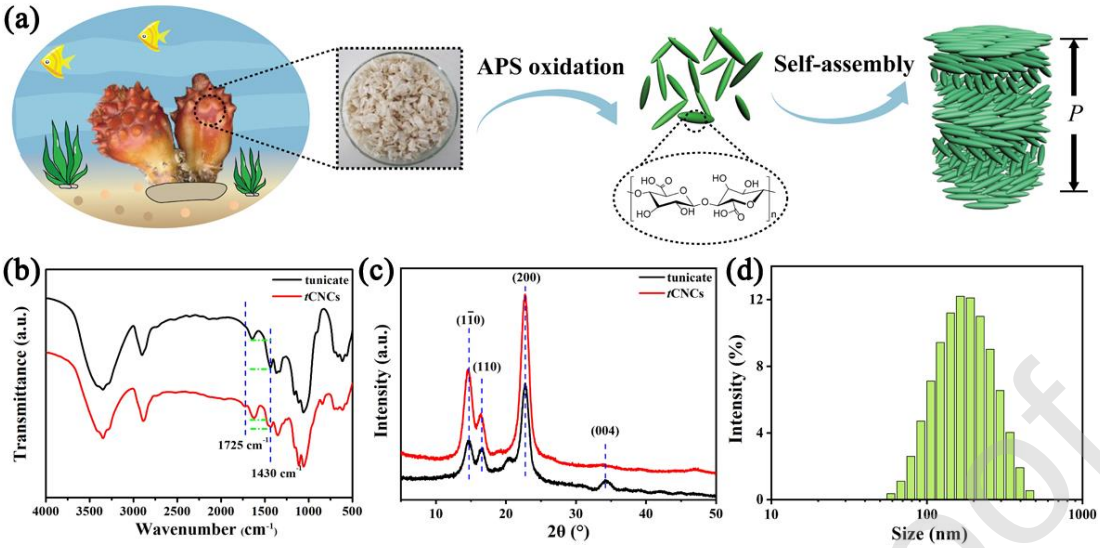

Fig.1 (a) Schematic illustration of the isolation and self-assembly of carboxylated *t*CNCs, (b) FT-IR spectra and (c) XRD patterns of carboxylated *t*CNCs and original tunicate cellulose, and (d) size distribution histogram of *t*CNCs suspension.

Cellulose was extracted from integumentary tissue the “tunic”, which covers the entire epidermis of the animal and acts as a skeletal structure. After alkali- and bleaching-treatment of tunic for several times, white product can be isolated, as is shown in Fig 1a. Then the modified *t*CNCs with carboxy group were fabricated through a simple one-step APS oxidation. The obtained *t*CNCs suspension was homogeneous, and which displayed enhanced transparency processed with subsequent ultrasonication. To further understand its properties, more characterizations were carried out.

Fig. 1b shows the FT-IR spectra of tunicate cellulose and carboxylated *t*CNCs that demonstrate the changes in chemical structure of cellulose before and after the oxidation. It is worth noting that the *t*CNCs sample shows a peak at 1725 cm^{-1},

corresponding to C=O stretching, which is absent for the untreated sample. The presence of C=O band indicates the sample was oxidized during treatment. Meanwhile, the absorption band intensity of the -CH_2 (1430 cm^{-1}) decreased significantly after the reaction, indicating the content of C6-CH_2 reduced (Castro-Guerrero & Gray, 2014). The data suggests that oxidation occurred preferentially at the C6 primary alcohol of crystalline cellulose, which is in accordance with the result of Luong et al (Leung et al., 2011).

As shown in Fig. 1c, the *t*CNCs exhibited typical cellulose I_β diffraction pattern with strong crystalline peaks at 14.6°, 16.4°, 22.8° and 34.2°, corresponding to the ($1\bar{1}0$), (110), (200) and (004) crystal planes, respectively. The result shows that the crystal structure of *t*CNCs was not destroyed after the APS oxidation. In addition, more intensive diffraction peaks of *t*CNCs can be observed compared to original tunicate cellulose. This is due to the amorphous region was removed by APS oxidation and the crystallinity was enhanced. Based on the Segal's equation, the crystallinity index (CrI) of *t*CNCs was determined. The obtained value of 86% is in good agreement with the CrI of CNCs prepared by APS oxidation (Castro-Guerrero & Gray, 2014). Furthermore, the crystallite size calculated from the Scherrer formula was 6.15 nm, similar to values found on literature (Filson, Dawson-Andoh, & Schwegler-Berry, 2009).

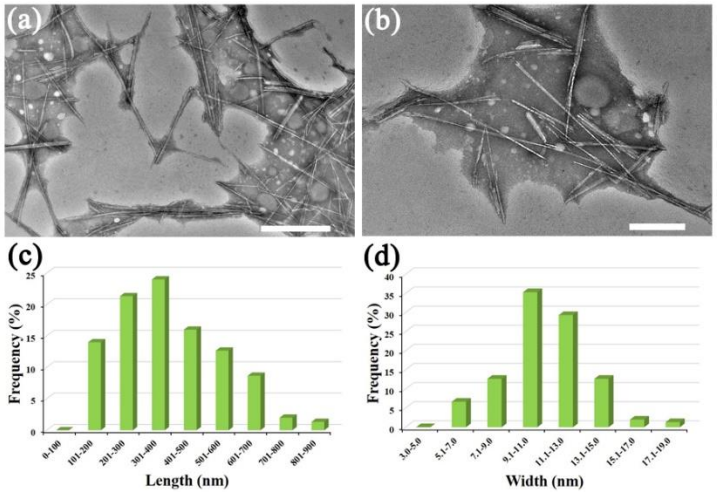

Fig.2 (a, b) TEM images of carboxylated *t*CNCs at different magnification and corresponding (b) length and (c) width statistical distribution histograms. (Scale bars are 500 and 200 nm in (a) and (b), respectively.)

As is well known, dimension of CNCs is of vital importance to the self-assembly. The size polydispersity of CNCs has an effect on their lyotropic liquid crystals behavior, so the precise control of size is essential. Fig. 1d shows the particle size distribution of *t*CNCs suspension from DLS measurement, which demonstrate that the distribution is relatively uniform with a polydispersity index (PDI) of 0.2. Besides, more detailed dimensional information was obtained from TEM images of carboxylated *t*CNCs, as is shown in Fig. 2. From the statistical histograms, it can be found that the dimension of *t*CNCs was evenly distributed, which is comparable to the above DLS results. The *t*CNCs have a length of 383 ± 164 nm and a width of 10.9 ± 2.3 nm calculated from 150 nanocrystals by using Nano Measurer software. Compared with the reported *t*CNCs (Tab.1), the length greatly decreased, which may be ascribed to the high-power ultrasonic post-processing. Accordingly, the uniform nanoscale dimensions will facilitate the self-assembly of carboxylated *t*CNCs.

Tab. 1 Size of A-*t*CNCs, H-*t*CNCs, A-*c*CNCs and corresponding critical concentration of phase separation.[a]

Samples	A-*t*CNCs	H-*t*CNCs[b]	A-*c*CNCs
Length	383 ± 164 nm	1300 ± 700 nm	145 ± 32 nm
Width	10.9 ± 2.3 nm	15-30 nm	7.5 ± 1.2 nm
Aspect ratio	40.2 ± 23.4	75 ± 65	20.5 ± 7.5
Critical concentration	3.5 wt%	0.5 wt%	4.1 wt%
Zeta potential	-43.5 mV	-	-40.5 mV

a A-*t*CNCs: APS oxidized tunicate CNCs, H-*t*CNCs: Sulfuric acid hydrolyzed tunicate CNCs, A-*c*CNCs: APS oxidized cotton CNCs.
b Referenced from Zhang et al., (2018) and Kimura et al., (2005).

From the conductimetric titration curve (Fig. S1), the *t*CNCs carboxyl content of 0.40 mmol/g was calculated. On the basis of the equation 2, the experimental degree of oxidation (DO) was 0.07. This value is close to the theoretical DO_{max} value of 0.1, indicating a high oxidation capacity of the APS oxidation method to tunicate cellulose (Habibi et al., 2006). After the oxidation treatment, carboxylate radical was introduced into the surface of cellulose, making *t*CNCs polyelectrolytic in natural state (Peng Liu, Oksman, & Mathew, 2016). Zeta potential is directly correlated to the surface charges density, and the value of -43.5 mV was obtained. High Zeta potential suggests that carboxylated *t*CNCs are well dispersed and the colloidal suspension is stable, which is of great significance to the formation of N*-LCs.

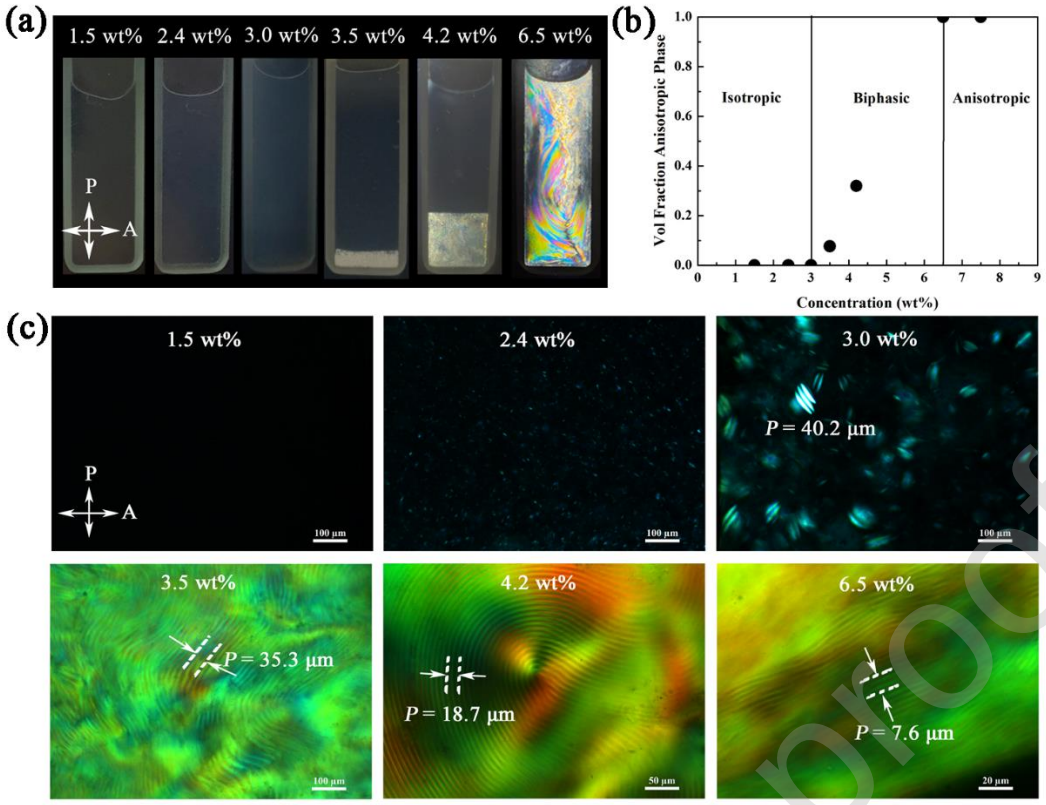

Fig.3 (a) Phase separation images of the carboxylated *t*CNCs suspensions with various concentrations in cuvettes, (b) corresponding phase transition diagram for *t*CNCs suspension, and (c) POM photographs of *t*CNCs suspensions with various concentrations (arrows indicating directions of the polarizer (P) and analyzer (A); samples were sandwiched between P and A)

It is generally known that the CNCs suspension with a low concentration exhibits a single isotropic phase. As the concentration exceeds a critical value, it will separate into two phases with an upper isotropic phase and an anisotropic bottom one. The critical concentration varies with the preparation methods and the sources of cellulose. To investigate the critical concentration, various concentrations of *t*CNCs suspensions were prepared. Fig. 3a shows the images of *t*CNCs suspensions with the concentrations of 1.5, 2.4, 3.0, 3.5, 4.2, and 6.5 wt% sandwiched between crossed

polarizers, respectively. The volume fraction of anisotropic phase was increased with the rising of suspension concentration. Dilute *t*CNCs suspensions (<3.5 wt%) displayed homogeneously isotropic, but with increasing concentration the suspension became biphasic (3.5-6.5 wt%) and then fully anisotropic (>6.5 wt%) as seen in the phase transition diagram (Fig. 3b). Rod-like *t*CNCs are randomly oriented at low concentration, then they form liquid crystals through the interparticle interaction when the concentration is above a critical value. Thus, it can be concluded that the critical concentration of phase separation for carboxylated *t*CNCs suspension is around 3.5 wt %. Recently, Zhang et al. (Zhang, Cheng, Chang, & Zhang, 2018) reported that *t*CNCs obtained from sulfuric acid hydrolysis has a critical concentration of 0.5 wt%, which is much lower than the above one. Based on the Onsager's phase separation theory that critical concentration decreased with increased aspect ratio (Beck-Candanedo, Roman, & Gray, 2005), the higher critical concentration of carboxylated *t*CNCs is ascribed to their smaller aspect ratio (Tab.1). Beyond that, the lyotropic liquid crystal behavior of carboxylated *c*CNCs was also investigated. From the TEM images (Fig. S2), *c*CNCs with length of 145 ± 32 nm and aspect ratio of 20.5 ± 7.5 were determined. Comparatively, both of parameters are smaller than those of *t*CNCs. In this circumstance, the critical concentration of 4.1 wt% and well-ordered fingerprint texture were observed for carboxylated *c*CNCs (Fig. S3 and S4).

The characteristic fingerprints of N*-LCs were also clearly observed, as is shown in Fig. 3c. The tactoids were firstly appeared at a concentration of 3.0 wt%, and then fingerprint texture emerged with the occurrence of phase separation. Remarkably, the

helical pitch decreased greatly from 40.2 to 7.6 μm as the concentration increased. The fingerprints texture of samples displayed good stability after being stored at 4℃ for 180 days, and the change of helical pitch was very small (less than 1 μm, Fig. S5). These phenomena demonstrate that carboxylated *t*CNCs have the ability to form lyotropic N*-LCs, which will further expand their applications in CNCs based chiral composites.

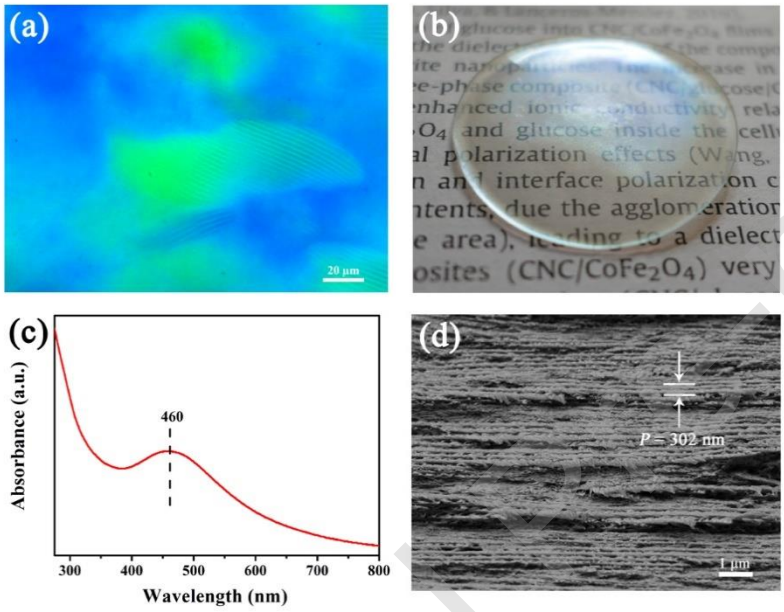

Fig. 4 (a) POM image of carboxylated *t*CNCs suspension during the evaporation process, (b) digital photo the iridescent *t*CNCs solid film, (c) UV–vis spectrum and (d) cross-sectional SEM image of *t*CNCs film.

The chiral nematic structure was retained in the carboxylated *t*CNCs solid film prepared by evaporation induced self-assembly. During the evaporation process, the fingerprint texture and birefringence were clearly observed with the concentration increased (Fig. 4a). After drying, solid film was prepared successfully, as shown in Fig. 4b, which showed excellent uniformity and transparency. To obtain more details,

optical property and fracture surface morphology of the film were characterized by UV-vis and SEM. Fig. 4c shows the UV–vis spectrum of the carboxylated *t*CNCs film, a peak at 460 nm was appeared that is ascribed to the selective reflection of helical structure in solid film. Meanwhile, highly ordered long-range layered structure was clearly observed from cross-sectional SEM image, as is shown in Fig 4d. The helical pitch was measured to be 302 nm, which is coincided with the calculated value ($P = \lambda / n_{avg}\sin\theta$ = 460/1.54 = 299 nm) obtained from optical spectroscopy and Bragg equation. The above results verify the chiral nematic structure was preserved in films, resulting in interesting optical properties.

4. Conclusion

In this work, carboxylated *t*CNCs with uniform nanoscale dimensions were fabricated from APS oxidation and ultrasonic treatment. For the first time, the formation of carboxylated *t*CNCs lyotropic N*-LCs was found, and the fingerprint texture was clearly observed. The critical concentration of phase separation for *t*CNCs suspension was around 3.5 wt%, which is lower than *c*CNCs. In addition, *t*CNCs solid film was prepared from evaporation induced self-assembly, indicating the chiral nematic structure was well preserved. These findings may bring new insight in the understanding of the self-assembly behavior of these systems that could be beneficial for the design of chiral functional materials and the development of abundant tunicate resources.

Credit Author Statement.docx

Jintao He: Conceptualization, Methodology, Data curation, Writing-Original draft, Writing-Reviewing & Editing.
Kaiqiang Bian: Conceptualization, Methodology, Data curation.
Guangzhe Piao: Resources, Supervision, Writing-Reviewing & Editing.

Acknowledgements

This work was partially supported by the Program for International Science & Technology Cooperation Projects of China (2011DFA50430).

References

Anglès, M. N., & Dufresne, A. (2000). Plasticized Starch/Tunicin Whiskers Nanocomposites. 1. Structural Analysis. *Macromolecules,* 33(22), 8344-8353.

Anglès, M. N., & Dufresne, A. (2001). Plasticized Starch/Tunicin Whiskers Nanocomposite Materials. 2. Mechanical Behavior. *Macromolecules,* 34(9), 2921-2931.

Azzam, F., Heux, L., & Jean, B. (2016). Adjustment of the Chiral Nematic Phase Properties of Cellulose Nanocrystals by Polymer Grafting. *Langmuir,* 32(17), 4305-4312.

Beck-Candanedo, S., Roman, M., & Gray, D. G. (2005). Effect of Reaction Conditions on the Properties and Behavior of Wood Cellulose Nanocrystal Suspensions. *Biomacromolecules,* 6(2), 1048-1054.

Castro-Guerrero, C. F., & Gray, D. G. (2014). Chiral nematic phase formation by aqueous suspensions of cellulose nanocrystals prepared by oxidation with ammonium persulfate. *Cellulose,* 21(4), 2567-2577.

Chen, W., Yu, H., Lee, S., Wei, T., Li, J., & Fan, Z. (2018). Nanocellulose: a promising nanomaterial for advanced electrochemical energy storage. *Chemical Society Reviews*, 47(8), 2837-2872.

Cheng, Q., Ye, D., Chang, C., & Zhang, L. (2017). Facile fabrication of superhydrophilic membranes consisted of fibrous tunicate cellulose nanocrystals for highly efficient oil/water separation. *Journal of Membrane Science*, 525, 1-8.

Chu, G., Camposeo, A., Vilensky, R., Vasilyev, G., Martin, P., Pisignano, D., & Zussman, E. (2019). Printing Flowers? Custom-Tailored Photonic Cellulose Films with Engineered Surface Topography. *Matter*, 1(4), 988-1000.

Chu, G., Vilensky, R., Vasilyev, G., Deng, S., Qu, D., Xu, Y., & Zussman, E. (2017). Structural Transition in Liquid Crystal Bubbles Generated from Fluidic Nanocellulose Colloids. *Angewandte Chemie International Edition*, 56(30), 8751-8755.

Filson, P. B., Dawson-Andoh, B. E., & Schwegler-Berry, D. (2009). Enzymatic-mediated production of cellulose nanocrystals from recycled pulp. *Green Chemistry*, 11(11), 1808-1814.

French, A. D., & Santiago Cintrón, M. (2013). Cellulose polymorphy, crystallite size, and the Segal Crystallinity Index. *Cellulose*, 20(1), 583-588.

Habibi, Y., Chanzy, H., & Vignon, M. R. (2006). TEMPO-mediated surface oxidation of cellulose whiskers. *Cellulose*, 13(6), 679-687.

He, J., Liu, S., Li, L., & Piao, G. (2017). Lyotropic liquid crystal behavior of

carboxylated cellulose nanocrystals. *Carbohydrate Polymers,* 164, 364-369.

Isogai, A., Saito, T., & Fukuzumi, H. (2011). TEMPO-oxidized cellulose nanofibers. *Nanoscale,* 3(1), 71-85.

Kaushik, M., & Moores, A. (2016). Review: nanocelluloses as versatile supports for metal nanoparticles and their applications in catalysis. *Green Chemistry,* 18(3), 622-637.

Kelly, J. A., Giese, M., Shopsowitz, K. E., Hamad, W. Y., & MacLachlan, M. J. (2014). The Development of Chiral Nematic Mesoporous Materials. *Accounts of Chemical Research,* 47(4), 1088-1096.

Kimura, F., Kimura, T., Tamura, M., Hirai, A., Ikuno, M., & Horii, F. (2005). Magnetic Alignment of the Chiral Nematic Phase of a Cellulose Microfibril Suspension. *Langmuir,* 21(5), 2034-2037.

Leung, A. C. W., Hrapovic, S., Lam, E., Liu, Y., Male, K. B., Mahmoud, K. A., & Luong, J. H. T. (2011). Characteristics and Properties of Carboxylated Cellulose Nanocrystals Prepared from a Novel One-Step Procedure. *Small,* 7(3), 302-305.

Liu, P., Oksman, K., & Mathew, A. P. (2016). Surface adsorption and self-assembly of Cu(II) ions on TEMPO-oxidized cellulose nanofibers in aqueous media. *Journal of Colloid and Interface Science,* 464, 175-182.

Liu, P., Pang, B., Dechert, S., Zhang, X., Andreas, L., Fischer, S., Meyer, F., & Zhang, K. (2020). Physical Structure Selectivity of Universal Alkaline Periodate Oxidation on Lignocellulose for Facile Isolation of Cellulose Nanocrystals.

Angewandte Chemie International Edition, 59, 3218-3225.

Liu, Y., Liu, L., Wang, K., Zhang, H., Yuan, Y., Wei, H., Wang, X., Duan, Y., Zhou, L., & Zhang, J. (2020). Modified ammonium persulfate oxidations for efficient preparation of carboxylated cellulose nanocrystals. *Carbohydrate Polymers*, 229, 115572.

Marchessault, R. H., Morehead, F. F., & Walter, N. M. (1959). Liquid Crystal Systems from Fibrillar Polysaccharides. *Nature*, 184(4686), 632-633.

Miao, C., & Hamad, W. Y. (2019). Critical insights into the reinforcement potential of cellulose nanocrystals in polymer nanocomposites. *Current Opinion in Solid State and Materials Science*, 23(4), 100761.

Moon, R. J., Martini, A., Nairn, J., Simonsen, J., & Youngblood, J. (2011). Cellulose nanomaterials review: structure, properties and nanocomposites. *Chemical Society Reviews*, 40(7), 3941-3994.

Nyström, G., Arcari, M., Adamcik, J., Usov, I., & Mezzenga, R. (2018). Nanocellulose Fragmentation Mechanisms and Inversion of Chirality from the Single Particle to the Cholesteric Phase. *ACS Nano*, 12(6), 5141-5148.

Oun, A. A., & Rhim, J.-W. (2017). Effect of oxidized chitin nanocrystals isolated by ammonium persulfate method on the properties of carboxymethyl cellulose-based films. *Carbohydrate Polymers*, 175, 712-720.

Oun, A. A., & Rhim, J.-W. (2018). Isolation of oxidized nanocellulose from rice straw using the ammonium persulfate method. *Cellulose*, 25(4), 2143-2149.

Pan, J., Hamad, W., & Straus, S. K. (2010). Parameters Affecting the Chiral Nematic

Phase of Nanocrystalline Cellulose Films. *Macromolecules,* 43(8), 3851-3858.

Reddy, N., & Yang, Y. (2005). Structure and properties of high quality natural cellulose fibers from cornstalks. *Polymer,* 46(15), 5494-5500.

Revol, J. F., Godbout, L., Dong, X., Gray, D. G., Chanzy, H., & Maret, G. (1994). Chiral nematic suspensions of cellulose crystallites; phase separation and magnetic field orientation. *Liquid Crystals,* 16(1), 127-134.

Revol, J. F., Bradford, H., Giasson, J., Marchessault, R. H., & Gray, D. G. (1992). Helicoidal self-ordering of cellulose microfibrils in aqueous suspension. *International Journal of Biological Macromolecules,* 14(3), 170-172.

Revol, J. F., Godbout, L., & Gray, D. (1998). Solid Self-Assembled Films of Cellulose with Chiral Nematic Order and Optically Variable Properties. *Journal of Pulp and Paper Science,* 24, 146-149.

Sacui, I. A., Nieuwendaal, R. C., Burnett, D. J., Stranick, S. J., Jorfi, M., Weder, C., Foster, E. J., Olsson, R. T., & Gilman, J. W. (2014). Comparison of the Properties of Cellulose Nanocrystals and Cellulose Nanofibrils Isolated from Bacteria, Tunicate, and Wood Processed Using Acid, Enzymatic, Mechanical, and Oxidative Methods. *ACS Applied Materials & Interfaces*, 6(9), 6127-6138.

Schütz, C., Van Rie, J., Eyley, S., Gençer, A., van Gorp, H., Rosenfeldt, S., Kang, K., & Thielemans, W. (2018). Effect of Source on the Properties and Behavior of Cellulose Nanocrystal Suspensions. *ACS Sustainable Chemistry & Engineering,* 6(7), 8317-8324.

Suopajärvi, T., Liimatainen, H., Hormi, O., & Niinimäki, J. (2013). Coagulation–flocculation treatment of municipal wastewater based on anionized nanocelluloses. *Chemical Engineering Journal,* 231, 59-67.

Thomas, B., Raj, M. C., B, A. K., H, R. M., Joy, J., Moores, A., Drisko, G. L., & Sanchez, C. (2018). Nanocellulose, a Versatile Green Platform: From Biosources to Materials and Their Applications. *Chemical Reviews,* 118(24), 11575-11625.

Trache, D., Hussin, M. H., Haafiz, M. K. M., & Thakur, V. K. (2017). Recent progress in cellulose nanocrystals: sources and production. *Nanoscale,* 9(5), 1763-1786.

Tran, A., Boott, C. E., & MacLachlan, M. J. (2020) Understanding the Self-Assembly of Cellulose Nanocrystals—Toward Chiral Photonic Materials. *Advanced Materials,* 1905876. DOI: 10.1002/adma.201905876.

Van Rie, J., Schütz, C., Gençer, A., Lombardo, S., Gasser, U., Kumar, S., Salazar-Alvarez, G., Kang, K., & Thielemans, W. (2019). Anisotropic Diffusion and Phase Behavior of Cellulose Nanocrystal Suspensions. *Langmuir,* 35(6), 2289-2302.

Wang, H., He, J., Zhang, M., Tam, K. C., & Ni, P. (2015). A new pathway towards polymer modified cellulose nanocrystals via a “grafting onto” process for drug delivery. *Polymer Chemistry,* 6(23), 4206-4209.

Yu, H., Chen, G., Wang, Y., & Yao, J. (2015). A facile one-pot route for preparing cellulose nanocrystal/zinc oxide nanohybrids with high antibacterial and photocatalytic activity. *Cellulose,* 22(1), 261-273.

Zhang, D., Zhang, Q., Gao, X., & Piao, G. (2013). A Nanocellulose Polypyrrole Composite Based on Tunicate Cellulose. *International Journal of Polymer Science*, 2013, 1-6.

Zhang, Y., Cheng, Q., Chang, C., & Zhang, L. (2018). Phase transition identification of cellulose nanocrystal suspensions derived from various raw materials. *Journal of Applied Polymer Science*, 135(24), 45702.

Zhao, Y., Zhang, Y., Lindström, M. E., & Li, J. (2015). Tunicate cellulose nanocrystals: Preparation, neat films and nanocomposite films with glucomannans. *Carbohydrate Polymers*, 117, 286-296.

Zhou, L., Li, N., Shu, J., Liu, Y., Wang, K., Cui, X., Yuan, Y., Ding, B., Geng, Y., Wang, Z., Duan, Y., & Zhang, J. (2018). One-Pot Preparation of Carboxylated Cellulose Nanocrystals and Their Liquid Crystalline Behaviors. *ACS Sustainable Chemistry & Engineering*, 6(9), 12403-12410.